THE ASTROPHYSICAL JOURNAL, 528:454–461, 2000 January 1

SIMULTANEOUS X-RAY AND RADIO MONITORING OF THE UNUSUAL BINARY LS I +61°303: MEASUREMENTS OF THE LIGHT CURVE AND HIGH-ENERGY SPECTRUM

F. A. HARRISON
Space Radiation Laboratory, California Institute of Technology, Pasadena, CA 91125; fiona@srl.caltech.edu
P. S. RAY
Code 7621 Space Science Division, Naval Research Laboratory, Washington, DC 20375; paulr@xeus.nrl.navy.mil
D. A. LEAHY
Department of Physics, University of Calgary, Calgary, AB T2N 1N4, Canada; leahy@iras.ucalgary.ca
E. B. WALTMAN
Code 7210 Remote Sensing Division, Naval Research Laboratory, Washington, DC 20375; waltmane@rsd.nrl.navy.mil
AND
G. G. POOLEY
Mullard Radio Astronomy Observatory, Cavendish Laboratory, Madingley Road, Cambridge CB3 0HE, England; ggp1@mrao.cam.ac.uk
Received 1999 April 8; accepted 1999 August 10

ABSTRACT

The binary system, LS I +61°303, is unusual both because of the dramatic, periodic, radio outbursts, and because of its possible association with the 100 MeV gamma-ray source, 2CG 135+01. We have performed simultaneous radio and *Rossi X-Ray Timing Explorer* X-ray observations at 11 intervals over the 26.5 day orbit, and in addition searched for variability on timescales ranging from milliseconds to hours. We confirm the modulation of the X-ray emission on orbital timescales originally reported by Taylor et al., and in addition we find a significant offset between the peak of the X-ray and radio flux. We argue that based on these results, the most likely X-ray emission mechanism is inverse Compton scattering of stellar photons off of electrons accelerated at the shock boundary between the relativistic wind of a young pulsar and the Be star wind. In these observations we also detected 2–150 keV flux from the nearby low-redshift quasar QSO 0241+622. Comparing these measurements to previous hard X-ray and gamma-ray observations of the region containing both LS I +61°303 and QSO 0241+622, it is clear that emission from the QSO dominates.

Subject headings: binaries: close — gamma rays: observations — radio continuum: stars — stars: individual (LS I +61°303)

1. INTRODUCTION

The Be binary system LS I +61°303 (associated with the radio source GT 0236+610) is remarkable for dramatic radio outbursts occurring with the 26.5 day orbital cycle (Gregory & Taylor 1978; Taylor & Gregory 1982), and for its possible association with the 100 MeV gamma-ray source 2CG 135+01 (Bignami & Hermsen 1983; Kniffen et al. 1997). Radio flares lasting several days occur every orbit, with the peak flux varying in phase by up to half the orbital cycle. The binary is a weak, variable X-ray source (Goldoni & Mereghetti 1995; Taylor et al. 1996; Leahy, Harrison, & Yoshida 1997) with a nonthermal spectrum. EGRET measurements indicate that the 100 MeV emission from the region may also be variable (Tavani et al. 1998). The gamma-ray error box contains no other likely counterparts. The gamma-ray localization is not, however, sufficiently accurate to make a secure association between 2CG 135+01 and LS I +61°303.

The mechanisms responsible for the radio outbursts and variable X-ray emission are not well understood. The radio emission is consistent with optically thin synchrotron radiation for most of the outburst, with indication that the source is self-absorbed at the beginning of the outburst rise (Taylor & Gregory 1984). The X-ray emission is consistent with either an extension of the radio synchrotron spectrum, or inverse Compton scattering of the stellar photons by the relativistic electrons responsible for the radio flux (Leahy, Harrison, & Yoshida 1997). The most plausible models proposed for the origin of the relativistic electrons are acceleration in a shock produced at the interaction of the Be star wind with the relativistic wind of a young pulsar companion (Maraschi & Treves 1981), or in a shock produced by the ejection of matter accreted onto a pulsar magnetosphere (Campana et al. 1995). In either case, both the X-ray and radio emission would vary with orbital phase.

In this paper, we present simultaneous *RXTE* X-ray, Green Bank Interferometer (GBI), and Ryle Telescope radio observations taken over a single orbital cycle. These observations provide a complete orbital light curve in 2–10 keV X-rays and 2.25, 8.3, and 15 GHz radio frequencies. On only one prior occasion has LS I +61°303 been monitored in the X-ray band over an entire orbital cycle (Taylor et al. 1996). We have also analyzed archival X-ray data and compiled a history of the X-ray variability. We have established X-ray flux variations on hourly timescales and have performed the most sensitive searches to date for rapid X-ray pulsations from the suggested neutron star companion. In addition, we have analyzed the 2–150 keV spectra of both LS I +61°303 and the nearby quasar QSO 0241+622, which has been included in the field of view of many previous hard X-ray measurements.

2. ORBITAL VARIABILITY

2.1. *RXTE Observations*

NASA's *Rossi X-ray Timing Explorer* (*RXTE*) carries two pointed instruments, the Proportional Counter Array

(PCA) and the High-Energy X-ray Timing Experiment (HEXTE). The PCA is an array of five nearly identical xenon proportional counter units (PCUs) sensitive to X-rays in the range 2–60 keV. The PCUs are co-aligned and collimated to a 1° field of view (FWHM). The total collecting area of the PCA is ~ 6300 cm^2. The HEXTE consists of two clusters of NaI/CsI phoswich scintillation counters sensitive in the range 15–250 keV. Each cluster has an effective area of ~ 800 cm^2. The clusters rock such that one is always pointed at the source, while the other monitors the background at a slightly offset point. The HEXTE collimators also have a field of view of 1° (FWHM).

We observed LS I +61°303 11 times with the PCA and HEXTE between 1996 March 1 and 1996 March 30, at intervals approximately equally spaced over the 26 day orbit. Several problems with the instruments affected our observations (which were made only 1 month after guest observations with RXTE began). On 1996 March 6, one of the four detectors in HEXTE cluster B failed. On 1996 March 19, PCUs 4 and 5 exhibited anomalous behavior, resulting in all five of the PCUs being shut down for one of our observations, and only three PCUs being active for the next. On 1996 March 25, the PCA gain was changed. The observation times are shown in Table 1, along with the radio phase, on-source integration time (total time minus SAA passages and Earth occultations), and number of active detectors.

Most previous papers on this source have defined the radio phase according to the ephemeris of Taylor & Gregory (1984). They defined an arbitrary phase zero of JD 2443366.775 and a period measured to be 26.496 ± 0.008 days based on data taken between 1977 and 1982. Using this ephemeris, the peak of the radio outbursts typically occurs around phase 0.6. More recently, Ray et al. (1997) found that radio outbursts monitored from 1994–1996 required using a period of 26.69 ± 0.02 days. They suggested that the orbital phase of the radio outbursts was varying in response to some other parameter in the system. In a Bayesian analysis of the complete 20 year data set Gregory, Peracaula, & Taylor (1999) find that the most favorable model for these data is a constant orbital period of 26.4917 ± 0.0025 days with a longer period of 1584^{+14}_{-11} days which modulates the typical outburst phase with a magnitude of 8 days and the flux between 100 and 300 mJy. In this paper we quote radio phase referring to this orbital ephemeris ($T_0 =$ JD 2,443,366.775, $P_{\rm orb} = 26.4917$ days). This allows a consistent treatment of current and historical observations. When appropriate, we will quote the predicted outburst phase from the long-term modulation analysis above.

2.2. *RXTE Analysis and Results*

2.2.1. *PCA*

We analyzed the PCA observations using the standard FTOOLS 4.0 package provided by the *RXTE* Guest Observer Facility (GOF). For most analyses not requiring high time resolution, we used the "Standard 2" mode data. This mode accumulates a single 129 channel spectrum from each detector anode every 16 s. These data are filtered by requiring that the PCUs be on, the source be more than 10° above the Earth's limb, and the spacecraft be pointed within 0.°02 of the source. Because the source is faint, and detected only at low energies, signal-to-noise is improved by taking data only from layer 1 of the PCUs. We then combined all of the selected data into one spectrum for each observation. Finally, a background spectrum is estimated and subtracted from the detected counts.

Because the PCA does not rock on and off source, to determine the background counting rate we rely on a parametrized model of the background, pcabackest v1.5 (Jahoda et al. 1998), provided by the *RXTE* GOF. This model includes three components: internal background which is a function of the instantaneous veto rate measured in the PCA, internal activation background which is a function of the time since the last SAA passage, and the cosmic diffuse flux in the 1° aperture which is an average of high Galactic latitude blank-sky pointings.

The top panel of Figure 1 shows the background-subtracted count rate in the 2–10 keV band for the 10 observations with useful PCA data. Source variability is evident, with a peak count rate occurring between radio phase 0.45–0.6. The second panel shows the X-ray flux, calculated from spectral fits to these data. Using XSPEC v10.00, we fitted the individual pointings with a power-law spectral model, with hydrogen column density fixed at the value measured by *ASCA* of 0.6×10^{22} cm^{-2} (Leahy et al. 1997). The fluxes were calculated by integrating this best-fit model from 2 to 10 keV.

The dominant error in the source variability and flux measurements is uncertainty in the background. Errors in estimating the time-variable internal background component will contribute to errors in determining the source

TABLE 1

OBSERVATION LOG OF *RXTE* OBSERVATIONS OF LS I +61°303, WITH FITTED FLUXES

Date UTC	Radio Phase	Number of PCUs	PCA Live Time (ks)	Flux (2–10 keV) ($\times 10^{-12}$ ergs cm^{-2} s^{-1})
1996 Mar 01 13:57–19:25.....	−0.17	5	8.9	8.4
1996 Mar 04 21:38–01:36.....	−0.04	5	9.3	12.1
1996 Mar 07 23:33–03:28.....	0.07	5	9.4	6.9
1996 Mar 10 01:07–05:02.....	0.15	5	9.1	6.5
1996 Mar 13 04:06–08:19.....	0.27	5	10.0	9.6
1996 Mar 16 00:54–06:06.....	0.38	5	9.5	13.2
1996 Mar 18 10:44–15:48.....	0.47	5	9.5	20.0
1996 Mar 20 23:19–03:06.....	0.58	0	0	NA
1996 Mar 24 07:55–13:10.....	0.69	3	11.0	12.2
1996 Mar 26 00:56–06:46.....	0.75	5	13.7	10.3
1996 Mar 30 04:07–10:40.....	0.91	5	14.6	9.2

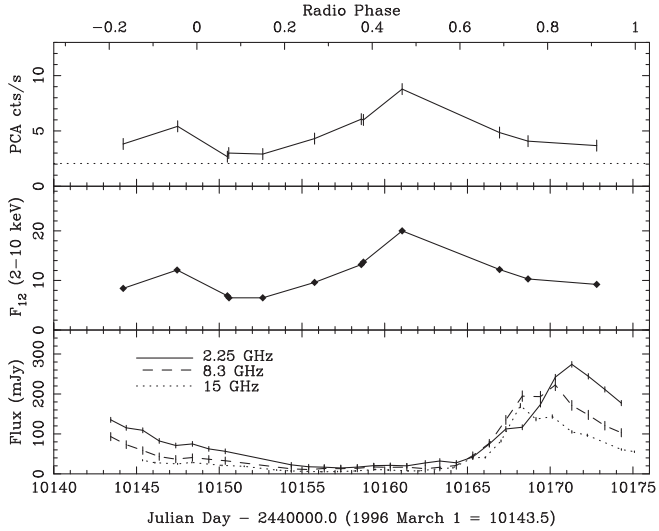

FIG. 1.—Comparison of *RXTE* PCA flux and radio flux during 1996 March. The top panel shows the PCA count rate (five PCUs, 2–10 keV, layer 1 only) for each observation. The dotted line shows the 2 σ upper limit to the error in the zero level due to errors in the model of the diffuse X-ray flux in the aperture (see text). The second panel shows the corresponding fitted 2–10 keV fluxes in units of 10^{-12} ergs cm^{-2} s^{-1}. The bottom panel shows the radio light curves at 2.25, 8.3, and 15 GHz measured quasi-simultaneously. Radio phase is defined in the text.

variability, while errors in determining the cosmic and Galactic diffuse flux contributions, or other X-ray sources in the FOV result in an uncertain zero level. To estimate errors in internal background determination, we produced background-subtracted count rate spectra for Earth-occulted data taken during our observations. Variations in the count rates are a measure of imperfect subtraction of the internal background components. We used the dispersion in these values to derive the systematic error bars on the individual observation count rates shown in Figure 1. These systematic errors dominate the statistical errors.

The horizontal dotted line in the top panel of Figure 1 shows the 2 σ upper limit in the uncertainty in zero level in the count rates due to the fact that the diffuse background may be different in the direction of LS I +61°303 than in the fields used for background subtraction. Two factors contribute to this uncertainty: variations of the diffuse cosmic background and any unaccounted for contribution from the diffuse Galactic ridge emission. The former contributes an estimated 0.6 counts s^{-1} (1 σ) uncertainty. This is determined from scaling the fluctuations measured by *HEAO-1* A-2 (Mushotzky & Jahoda 1992), correcting by the square root of the ratio of the *HEAO-1* A-2 to PCA beam sizes. We derive an upper limit of 0.5 counts s^{-1} (1 σ) to any contribution from diffuse Galactic ridge emission in two separate ways. First, the upper limit from *HEAO-1* A-2 presented in Worrall et al. (1982) toward this direction gives an upper limit of 0.4 counts s^{-1}, which compares well to the 0.5 counts s^{-1} upper limit derived from PCA slew data taken from a 0°.5–2° annulus around LS I +61°303.

Confusion from other X-ray sources in the FOV is not a problem in this field. The two sources found in the *ROSAT* sky survey within the PCA field of view are both stellar sources with soft spectra which, based on spectral fits, contribute less than 0.1 counts s^{-1} in the PCA. One of these sources, identified with the stellar source BD 60536, was also detected with *ASCA*, which found a thermal spectrum with temperature 0.8 keV (Leahy et al. 1997).

2.2.2. *HEXTE*

During the observations the two HEXTE clusters were configured to alternately point on-source and at four separate background regions 1°.5 away. The HEXTE data analysis proceeded as follows. We first selected events by which field the cluster was viewing. We then extracted spectra for each field. At this point, we corrected the exposure times for each spectrum to account for the dead time in the HEXTE detector using hxtdead v0.0.1. Due to electronics problems, the dead time is much larger than was expected before launch.

During six of the 11 observations, one of the background regions contained the quasar QSO 0241+622 within the field of view of the HEXTE collimator. This QSO is a known hard X-ray source (Turner & Pounds 1989) and many previous hard X-ray observations of the region made using nonimaging instruments have been unable to conclusively determine whether LS I +61°303 or the QSO is the source of the measured flux. Figure 2 shows the four background locations, labeled as $A \pm 1°.5$ and $B \pm 1°.5$ during pointing 7, showing the position of QSO 0241+622 (indicated by a star) just outside the FWHM FOV of background region $A + 1°.5$. By using one of the other three fields that do not contain any known hard X-ray source as background fields, we were able to derive flux measurements both for LS I +61°303 and for QSO 0241+622. We did not use the $A + 1°.5$ field as a background for the LS I +61°303 pointings.

LS I +61°303 is not bright enough in the HEXTE band to obtain significant detections for the individual pointings. We therefore summed data from all pointings, totaling 69.8

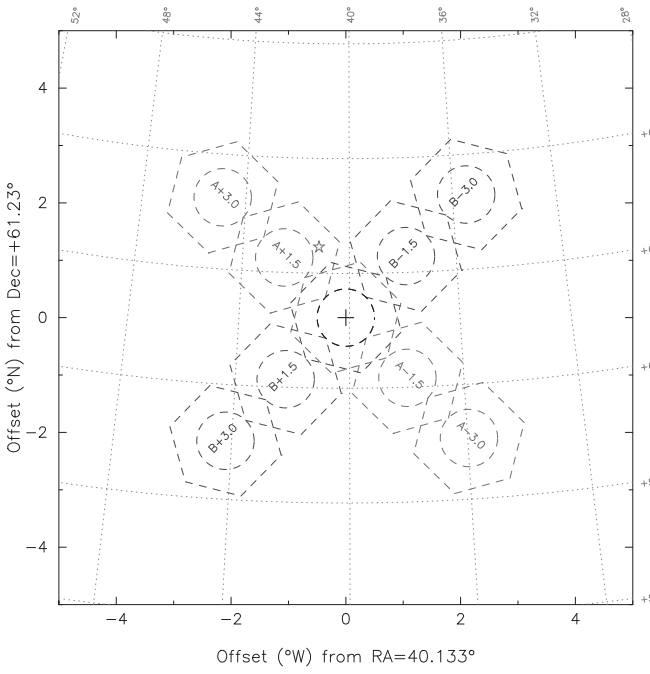

FIG. 2.—Orientation of the HEXTE background fields during observation 7 (1996 March 18 UT +00:00, R.A. = 40°.133, decl. = +61°.23, roll offset = +0°.0) The star shows the position of the quasar QSO 0241+662 which was contained in one of the background fields, $A + 1.5$. The orientation of the fields varied between pointings.

ks on source after deadtime correction, to search for high-energy emission. LS I +61°303 is detected at the 6.7 σ level in the 15–150 keV band in the summed data set (0.45 ± 0.1 counts s^{-1} in Cluster A and 0.37 ± 0.07 counts s^{-1} in Cluster B). We also divided the observations into two sets, set L consisting of pointings 3, 4, 10, and 11, when the measured PCA flux was low (below the mean), and set H consisting of pointings 6–9 when the measured PCA flux was high. In set L, we did not find a significant detection of the source, with a 15–150 keV count rate of -0.014 ± 0.15 in Cluster A and 0.21 ± 0.11 counts s^{-1} in Cluster B. In set H, however, we measured a positive count rate in the 15–150 keV band of 0.86 ± 0.16 in Cluster A and 0.49 ± 0.11 in Cluster B, a detection at the 7 σ level. This gives further confidence that the measured hard X-ray flux is associated with LS I +61°303 and is modulated on the same timescale as the soft emission. For set H, model fitting with XSPEC using a power-law spectral model yields a flux of 9×10^{-11} ergs cm^{-2} s^{-1} in the 15–150 keV band.

For QSO 0241+622, we summed data from pointings 6–11, during which the quasar was in field $A + 1\overset{\circ}{.}5$ and within $0\overset{\circ}{.}7$ of the field center. Using field $A - 1\overset{\circ}{.}5$ to determine the background, we detect the quasar at a significance level of 5.3 σ in the 15–150 keV band, with a count rate in the instrument of 0.85 ± 0.16. We also summed data from pointings 1–5, when the quasar was further than $0\overset{\circ}{.}7$ from the field center. Using the same technique we find a count rate consistent with zero of 0.21 ± 0.17. Correcting for the collimator response, and using XSPEC to fit a power-law to pointings 6–11, we find a hard X-ray flux for QSO 0241+622 of 2.0×10^{-10} ergs cm^{-2} s^{-2} (15–150 keV). We find a power-law photon spectral index of 1.2–2.2, but this may be modified by the collimator somewhat. Given the limited statistics of the detection, applying an energy-dependent collimator correction is not warranted.

To further confirm the detection of QSO 0241+622, we obtained a 10 ks observation of the source taken 1997 October 21 from the public archive and analyzed the PCA data (the observation is too short for a significant HEXTE detection). QSO 0241+622 is positively detected in this pointing, with a PCA 2–10 keV count rate of about 11 counts s^{-1} in three PCUs. The background estimate for this period is much better than for the 1996 March observations due to a recent background model developed by the PCA team which is applicable to gain epoch 3. Model fitting with an absorbed power law plus Gaussian iron line at 6.1 keV yields an excellent fit (reduced χ^2 of 0.6 when fitting Standard2 channels 3 to 38). The best-fit power-law spectral index is 1.73 ± 0.05 with normalization of 0.009 ± 0.001 γ cm^{-2} s^{-1} keV^{-1} at 1 keV. The corresponding 2–10 keV flux is 3.6×10^{-11} ergs cm^{-2} s^{-1}. Extrapolating this fit into the 15–150 keV HEXTE band yields a flux of 1.0×10^{-10} ergs cm^{-2} s^{-1}, reasonably close to our off-axis HEXTE observation considering the possibility of source variability, and the rough collimator correction and poor statistics of our HEXTE measurement. The measured flux and spectral index are fully consistent with the earlier *EXOSAT* measurement of 3.7×10^{-11} ergs cm^{-2} s^{-1} (2–10 keV) and spectral index of $1.70^{+0.27}_{-0.18}$ (Turner & Pounds 1989).

2.3. *Radio Data Analysis and Results*

Throughout the entire binary orbit coincident with the *RXTE* pointings, we monitored the source frequently using the two-element Green Bank Interferometer (GBI) in West Virginia and the Ryle telescope in Cambridge, England. The GBI consists of two 26 m antennas each of which has a pair of cooled receivers which simultaneously receive signals at 2.25 and 8.3 GHz with a system bandwidth of 35 MHz. Each observation consists of a 10 minute scan. Measured correlator amplitudes are converted to fluxes by comparing to standard, regularly observed calibrators. Constraints imposed by the radio telescope mount and elevation angle of the source precluded strict simultaneity of the X-ray and radio observations; however, radio observations were performed closely prior to and following the *RXTE* pointings. Details of the data analysis and error estimation for GBI monitoring of LS I +61°303 were presented by Ray et al. (1997).

The Ryle Telescope is an eight-element radio interferometer. Each element is a 13 m Cassegrain antenna. Throughout the observations described here, the instrument operated at 15 GHz with a bandwidth of 350 MHz. The rms noise on a 5 minute integration is about 1.7 mJy, although this degrades in poor weather. When the source is bright, the overall flux calibration will be the dominant error; and rms deviation of 3% has been established empirically for these circumstances. Observations of a calibration source (4C 67.05) are interleaved with observations of LS I +61°303.

The bottom panel of Figure 1 shows the three-frequency radio data for the orbital cycle coincident with the *RXTE* pointings. As seen previously by Ray et al. (1997), these data show a clear progression from an approximately flat spectrum to an optically thin spectrum during the outburst.

2.4. *Archival Data*

LS I +61°303 has been simultaneously monitored at both X-ray and radio wavelengths on two other occasions, once with *ROSAT*/VLA (Taylor et al. 1996), and once with *ASCA*/GBI (Leahy et al. 1997). In order to compare the variability seen with *RXTE*, we have reanalyzed these data, using the updated ephemeris. In the case of *ROSAT*, we reduced the X-ray data using the accurate column depth measured by *ASCA* and a power-law model to derive the flux. The GBI data taken simultaneously with the *ASCA* measurements have not been previously presented.

2.4.1. *ASCA*

The source was observed twice during the same orbit by *ASCA*. The first observation took place on 1994 February 3 (MJD 49386) beginning at 7:34 UT and ending at 11:01 UT, and the second observation began on 1994 February 9 (MJD 49392) at 7:34 UT and ended on the same day at 17:08 UT. Throughout the radio outburst coincident with the *ASCA* pointings, we monitored the source using the Green Bank Interferometer (GBI) at 2.25 and 8.3 GHz. During the quiescent radio state LS I +61°303 was monitored every two days, and during the radio outburst the source was monitored 2–4 times every day. Each observation consists of a 10 minute scan, during which both frequencies are monitored simultaneously.

Using the updated ephemeris, the *ASCA* pointings occurred at phases 0.23 and 0.47. Figure 3 shows the X-ray fluxes for the two pointings plotted with the radio data taken during the same outburst. Derivation of the flux values was presented by Leahy et al. (1997).

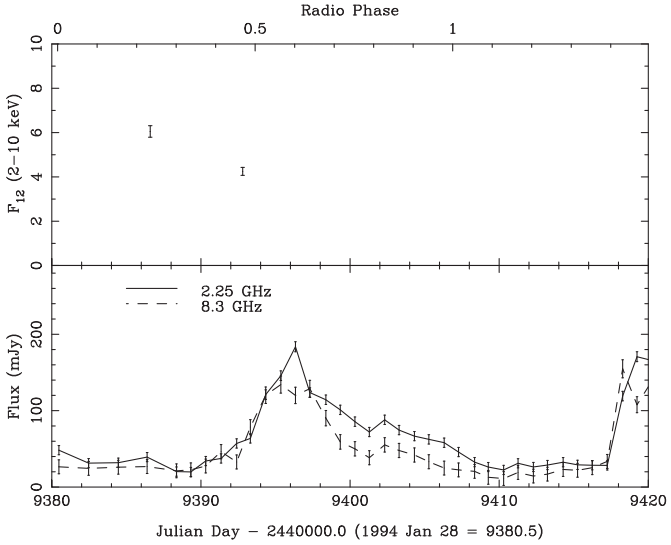

FIG. 3.—Two-frequency radio light curve (*bottom*) taken simultaneously with the two *ASCA* pointings (flux levels shown in the top panel). All error bars are 1 σ.

2.4.2. *ROSAT*

Taylor et al. (1996) observed LS I $+61°303$ on nine occasions over an orbital cycle with *ROSAT*, and also with the VLA at 5 GHz on 10 occasions during the same outburst. We have replotted their radio data, correcting for the updated ephemeris, in Figure 4. The X-ray flux points in this plot are based on a reanalysis of data retrieved from the public archive. From the *ASCA* observations, it is now clear that the spectrum is a power law, and an accurate column depth has been derived. For fitting the X-ray data, we allowed the power-law spectral index to vary, but fixed the column density at the *ASCA* value of 0.6×10^{22} cm^{-2} (Leahy et al. 1997). The X-ray flux is also plotted in Figure 4.

3. SHORT-TERM VARIABILITY

Small amplitude flares with timescales for rise and fall of ~ 1.5 hr have been observed in the radio (Peracaula 1997).

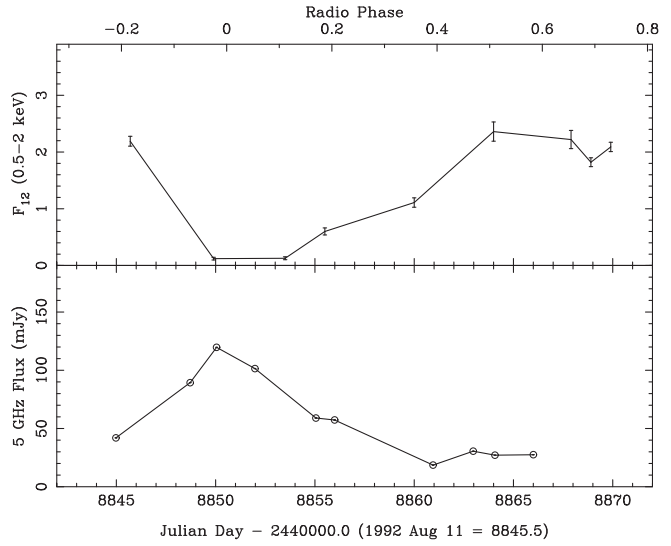

FIG. 4.—*ROSAT* light curve from one radio outburst cycle (*top*) and the 5 GHz radio data taken at the VLA during the same cycle (*bottom*).

We searched for similar variability in the archival data. The *ROSAT* data were very sparsely sampled, with the pointings being interrupted by long data gaps. It was therefore not possible to search for variability on hour timescales. Background variations on 90 minute orbital timescales in the *RXTE* PCA data also preclude searching for this periodicity in these data. The two *ASCA* pointings were interrupted only by Earth occultations and SAA passage, and we searched for variability in the count rates in the two GIS detectors. We found that during the first pointing (P1) the flux is consistent with a constant value; however, during the second (P2) the X-ray emission is variable on similar timescales to those seen in the radio, but with relatively large amplitude. Figure 5 shows light curves, binned in 5 minute intervals, from the two GIS detectors combined for the two pointings. The variability by more than 50% is evident in the second data set. The short gaps in the light curves are due to passage through the South Atlantic Anomaly and Earth occultations.

In order to search for smaller amplitude variability during P1, and characterize the fastest time scales of the variability seen during P2, we used a Lomb normalized periodogram (Press et al. 1992, p. 575, and references therein). This technique does not introduce features due to data gaps (such as SAA passages and Earth occultations) which would normally appear using standard Fourier analysis, since the data are evaluated only at times when they are actually measured. A periodogram of the data from P1 indicates no power at any frequency up to the Nyquist frequency and is entirely consistent with Poisson noise. Highly significant power is, however, seen in the data from P2 with the highest frequency of 10^{-4} s^{-1}, indicating variability on timescales of ~ 40 minutes. This implies a limit on the characteristic size for the emission region of $\lesssim 6 \times 10^{13}$ cm, or ~ 4 AU.

3.1. *Periodicity Searches*

Several models for the behavior of this source invoke a rapidly spinning, magnetized neutron star. If such a star is present, and if at least some of the X-ray emission observed originates within the magnetosphere of this neutron star, then we expect to find modulation of the X-ray flux at the

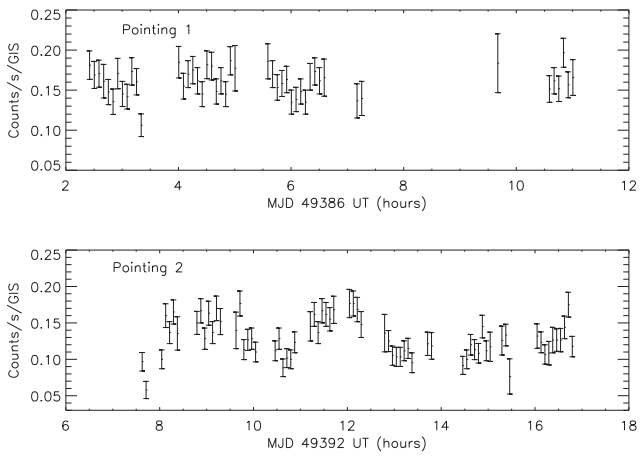

FIG. 5.—Count rate in the 1–5 keV band from LS I $+6°303$ for the two *ASCA* pointings. The first pointing is consistent with no variability on any timescale, whereas during the second pointing the source varies by $\sim 50\%$ on timescales of 30 minutes. Error bars are 1 σ.

neutron star rotation period. We have searched both the *RXTE* and *ASCA* data for coherent pulsations.

3.1.1. *RXTE*

We searched each section of nearly continuous data (a total of 36 observations, typically 1000–4000 s long) independently for evidence of coherent periodicities. For this search we used the "GoodXenon" data, which retain full time resolution (1 μs) and energy information about every nonvetoed X-ray photon. We selected these data for good time intervals, events in the 2–10 keV range, and in layer 1 only. We then corrected event times to the Solar System Barycenter so that Doppler shifts from the motion of the Earth and the spacecraft would not smear out a coherent signal from the source. We generated light curves with 1 ms resolution (1–4 $\times$ 10^6 bins).

Because the neutron star is being accelerated in its orbit around the companion B star, a search over orbital acceleration is required to keep short-period pulsars from being rendered undetectable due their period changing during the observation. Thus, we applied a range of orbital accelerations to the time series before performing the standard pulsar search. This consists of doing a Fast Fourier Transform, generating a normalized power spectrum, and searching for narrow significant peaks both singly and in harmonically related groups. We found no significant peaks in the range 0.01–500 Hz in any of the observations down to a pulsed fraction of $\sim$6% for an individual 1000 s data segment.

Finally, to improve the sensitivity of the search to slow pulsars (>a few hundred ms) for which orbital acceleration is negligible, we averaged all 36 unaccelerated power spectra and searched for peaks. Again, no significant periodicities were found. This search was sensitive to a pulsed fraction of $\sim$1%. In both cases, pulsed fractions are calculated for a sinusoidal modulation and the fraction is the fraction of the *total* count rate (including source, cosmic background, and instrumental background).

As a test of the *RXTE* extraction software and of our pulsation search code, we extracted data from the known rotation-powered X-ray pulsar PSR 1509−58 which was taken during the *RXTE* In Orbit Checkout period and is part of the *RXTE* public archive. The GoodXenon data from a 2000 s observation of PSR 1509−58 was then subjected to the same filtering, barycentering and processing as the data from LS I +61°303. The 6.627 Hz pulsation and at least three harmonics were easily detected at a significance of 58 σ.

3.1.2. *ASCA*

In addition to the *RXTE* search, we performed a pulsation search on the *ASCA* data. For the GIS detectors during P1 the time resolution of 0.0625 s limits the search to a minimum period of 0.125 s, and for P2, the minimum period searched is 1.0 s, corresponding to the Nyquist limit for the 0.5 s sampling. Epoch folding using the standard XRONOS software (available from the High Energy Astrophysics Science Archive Research Center (HEASARC) at Goddard Space Flight Center) failed to detect periodicity in either pointing. Table 2 summarizes the 90% confidence upper limits on the amplitude of pulsed emission for searches on the separate and combined GIS 1 and 2 data. We calculated these limits using the formalism described in Leahy et al. (1983). A second source in the *ASCA* FOV, identified as a stellar source (labeled Source2) was also searched for pulsations, and the upper limits are also given in Table 1. For P1, in addition to the epoch folding, we performed an FFT, which yielded nearly identical upper limits on the pulsed amplitude fraction as the epoch folding. For P2, aperiodic variability in the source precluded the use of an FFT for period searching (see § 3). We also searched the SIS data to a minimum period of 8 s, (determined by the 4 s CCD readout time), and found no pulsations, with limits similar to those presented for the GIS.

TABLE 2

ASCA PERIODICITY SEARCH LIMITS

	P1		P2	
DETECTOR	Number of Events	Amplitude Limit	Number of Events	Amplitude Limit
		LS I +61°303		
GIS 1	2638	0.28	2159	0.24
GIS 2	2629	0.28	2585	0.22
GIS 1 + 2.....	5267	0.20	4744	0.16
		Source 2		
GIS 1	455	0.68	690	0.42
GIS 2	434	0.70	738	0.40
GIS 1 + 2.....	889	0.49	1428	0.29

To search for short-period pulsations, for which smearing of the pulsed signal due to variable Doppler shifts resulting from the binary orbital motion can be important, we performed an acceleration search on the GIS data from P1. The variation in the pulse frequency is well-approximated by a linear trend over the duration of each observation. We searched a range of constant frequency derivatives from -3.6×10^{-7} s^{-2} $< \dot{\nu} <$ 3.6×10^{-7} s^{-2} (consistent with the range expected from the orbital solutions) in 1600 spacings. No periodicity was detected.

4. DISCUSSION

Several common characteristics of the two simultaneous, well-sampled X-ray and radio light curves (Figs. 1 and 4) are evident. Both are clearly modulated at the orbital period, and the peak in the X-ray emission is significantly offset (by 0.4–0.5 in phase) from the peak in the radio emission. Although containing only two data points, the *ASCA* observations are also consistent with the anticorrelation of radio and X-ray emission. In the *ROSAT* 0.5–2 keV data, the ratio of peak to quiescent luminosity is a factor $\sim$20, similar to what is observed in the radio, while in the *RXTE*/PCA 2–10 keV data, the variation is a factor 3–7 (the range depending on the uncertain zero point). Because of the poor spectral resolution and narrow bandpass of the *ROSAT* data, and the difficulty in determining spectral parameters in the *RXTE*/PCA data, it is impossible to determine if this difference arises from variable X-ray absorption (potentially important in the soft *ROSAT* band but negligible for the PCA), variation in the spectral index, or variation in the X-ray outburst intensity orbit-to-orbit.

These observations suggest that it is unlikely that both the X-ray and the radio flux arise from synchrotron emission from a common electron population. Rather, it is more likely that the X-ray flux results from inverse Compton scattering of stellar photons off a quasi-steady relativistic

electron population. First, it is difficult to accommodate a significant offset between the X-ray and radio peaks if both result from synchrotron emission from a common population. Furthermore, for reasonable synchrotron models for the radio emission, inverse Compton losses should dominate at X-ray wavelengths over the entire orbit. For example, Peracaula (1997) has modeled the synchrotron emission from an expanding spherical plasmon ejected from the binary system to explain the radio emission. To fit these data, the initial radius is $r_0 = 1.5 \times 10^{13}$ cm, the distance from the star is the orbital separation ($a = 7. \times 10^{12}$ cm), the magnetic field is $B = 0.15$ G, and the expansion velocity is 3×10^7 cm s^{-1}. Electrons are injected uniformly into the expanding sphere at a steady rate over 7 days. In this model, to get the radio rise requires a large initial r_0, and for the implied magnetic field and r_0, inverse Compton losses will dominate over synchrotron losses at all distances from the star. For synchrotron losses to be important at X-ray energies requires $B \gtrsim 300$ G for an electron population with spectral index 2.1 (steeper spectral index requires a higher field).

The small-amplitude of the orbital modulation of the X-ray flux relative to the radio observed by *RXTE* indicates that the electron population responsible for the inverse Compton emission is relatively constant, with the flux modulation likely resulting from variations in the stellar photon density as a function of position in an eccentric orbit. The X-ray maximum will occur near periastron, where the stellar photon density is highest (although some offset is possible if the Be star equator is not aligned with the orbit). The factor 3–6 X-ray variations would imply $r_{\rm min}/r_{\rm max} = 1/\sqrt{3}$–$1/\sqrt{6}$, or orbital eccentricity $\epsilon = 0.27$–0.42 for a steady electron population. This range is consistent with the poorly defined orbital parameters, which allow a range of eccentricity from 0.2–0.8 (Hutchings & Crampton 1981).

As originally proposed by Marashi & Treves (1981), a relatively steady electron population could be produced at the shock resulting from the interaction of the relativistic wind of a young pulsar with the Be stellar wind. The pulsar wind would create a cavity, with the boundary determined by dynamic pressure balance. These electrons inverse Compton scatter the stellar photons, producing X-ray emission, modulated by the variation in photon flux due to an eccentric orbit. The observed 2–10 keV X-ray luminosity of $(1$–$6) \times 10^{33}[D/(2.3\ {\rm kpc})]^2$ ergs s^{-1} is consistent with the shock interpretation and is similar to the observed luminosity near periastron of PSR B1259−63 (Kaspi et al. 1995), for which a similar mechanism has been invoked (Tavani, Arons, & Kaspi 1994). This model is also consistent with the lack of observed X-ray pulsations, since the X-ray emission is produced well outside the pulsar magnetosphere.

To explain the periodic radio outbursts requires an expanding plasmon. This could be produced when, sometime after periastron, the stellar wind pressure at the back side of the cavity becomes low enough that the cavity is no longer closed, allowing relativistic particles to stream away from the system, producing the radio emission and the observed expanding VLBI source. In this scenario, the X-ray peak should occur at periastron, and the radio outburst approximately 0.5 in phase away, as is observed. If 2CG 135+01 is associated with the system, the 100 MeV gamma-rays could also be produced via the inverse Compton mechanism by electrons of energy $\sim 3 \times 10^{-3}$ ergs. This emission should also be modulated at the orbital period. The EGRET flux from 2CG 135+01 is, in fact, time variable on day timescales (Tavani et al. 1998); however, the statistics are not sufficient to establish an orbital modulation.

4.1. *High-Energy Spectrum*

Numerous instruments have claimed detection of LS I +61°303 at hard X-ray and gamma-ray energies; however, few have had positioning capability sufficient to distinguish between emission from the binary and QSO 0241+622 (QSO 0241+622 being the only source within a several degree radius with a known hard spectrum).

Figure 6 summarizes some of the most secure hard X-ray and gamma-ray detections from this region. As described previously, the PCA and HEXTE clearly detect both sources. In the PCA, the quasar 2–10 keV flux is a factor ~2 higher than the average high-state of LS I +61°303. In HEXTE, the quasar 15–40 keV flux (determined at a different epoch than the PCA quasar measurement) is a factor 2–7 higher than the HEXTE LS I +61°303 detection. This would tend to indicate variability of the QSO; however, the statistics are limited. To derive PCA fluxes for LS I +61°303, given the uncertainties in the PCA background subtraction and response for the pointing, we fit a power-law model with photon index 1.8 (consistent with the *ASCA* values), and we show a range that includes uncertainty in the zero level. For the HEXTE quasar detection, we used the standard background subtraction and fitted a flat spectrum over the 15–40 keV band to determine the flux. The OSSE and COMPTEL measurements shown in the figure included both LS I +61°303 and QSO 0241+622 in the

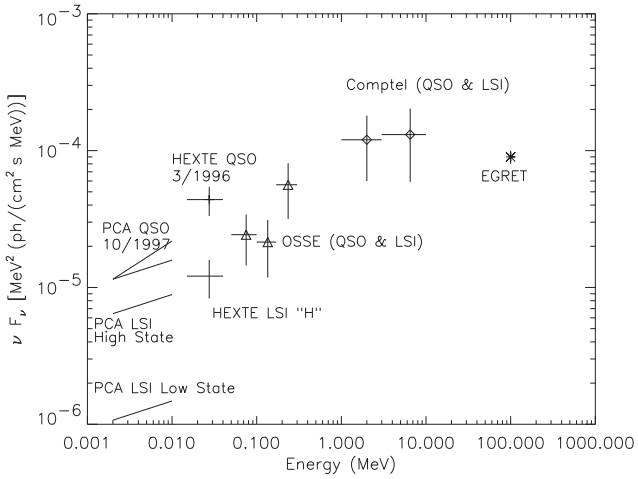

FIG. 6.—Compilation of selected high-energy observations of the region containing LS I +61°303 and QSO 0241+662. Previous observations in the 100 keV–MeV band by OSSE (*triangles*) (Strickman et al. 1998) and COMPTEL (*diamonds*) (van Dijk et al. 1996) included both LS I +61°303 and QSO 0241+662, while *RXTE* resolved both sources in the 2–150 keV band. The range of 2–10 flux for LS I +61°303 indicates the variation from high-state to low state, and includes in the range uncertain background subtraction. It is clear that the OSSE and COMPTEL measurements are dominated by flux from QSO 0241+662, since the observation periods are long, and average over a large fraction of the LS I +61°303 orbit. The EGRET observation (Kniffen et al. 1997) excludes emission from QSO 0241+662, but the 13′ error radius makes association with LS I +61°303 uncertain.

instrument fields of view (Strickman et al. 1998; van Dijk et al. 1996). The EGRET angular resolution is sufficient to exclude the quasar as the source of the gamma-ray emission (but the 13′ error radius makes positive association of the 100 MeV flux with LS I +61°303 uncertain).

It is clear from the *RXTE* observations that both the OSSE and COMPTEL measurements were dominated by flux from the quasar. Both observations integrated over times comparable to the LS I +61°303 orbit, and should be consistent with the average LS I +61°303 flux, which is a factor ∼5 lower than the QSO flux.

5. CONCLUSIONS

Our observations have confirmed that the X-ray and soft gamma-ray emission from LS I +61°303 is variable, and modulated on the orbital timescale. The *RXTE* observations sample a harder band than the previous *ROSAT* data, and we can eliminate variable absorption as the source of the flux modulation. From the two well-sampled light curves, it is clear that the X-ray emission peaks almost half an orbit before the radio. One explanation for this offset is that the high-energy emission is produced by inverse Compton scattering of stellar photons by a population of relativistic electrons produced at a nearly steady rate at the shock interaction of the relativistic wind of a young pulsar and the Be star wind. This would produce an X-ray peak near periastron. The synchrotron radio emission would then arise from the expansion of the plasma near apastron, when the cavity produced by the pulsar is no longer confined. Our observations fail to detect X-ray pulsations that would signify the presence of a young neutron star.

We also detected X-ray emission from the nearby QSO 0241+622 in the 2–150 keV band. The quasar is an approximate factor of 2 brighter than the average high-state LS I +61°303 flux at these energies. Previous 100 keV–MeV observations of the field made by OSSE and COMPTEL were therefore likely dominated by the quasar emission. The broadband 1 keV–100 MeV spectrum of LS I +61°303 therefore remains uncertain. Future high-energy missions, such as *GLAST*, will have the angular resolution and flux sensitivity both to positionally associate 2CG 135+01 and LS I +61°303 and to detect orbital modulation in the 100 MeV flux, if it exists.

We would like to thank Keith Jahoda and the *RXTE* GOF staff for assistance with the *RXTE* software and background models. Portions of this work were funded by NASA under the *RXTE* Guest Investigator program. Basic research in X-ray and Radio Astronomy at the Naval Research Laboratory is supported by the Office of Naval Research.

REFERENCES

Bignami, G. F. B., & Hermsen, W. 1983, ARA&A, 21, 67
Campana, S., Stella, L., Mereghetti, S., & Colpi, M. 1995, A&A, 297, 385
Goldoni, P., & Mereghetti, S. 1995, A&A, 299, 751
Gregory, P. C., Peracaula, M., & Taylor, A. R. 1999, ApJ, 520, 376
Gregory, P. C., & Taylor, A. R. 1978, Nature, 272, 704
Hutchings, J. B., & Crampton, D. 1981, PASP, 93, 486
Jahoda, K., et al. 1998, preprint
Kaspi, V. M., Tavani, M., Nagase, F., Hirayama, M., Hoshino, M., Aoki, T., Kawai, N., & Arons, J. 1995, ApJ, 453, 424
Kniffen, D. A., et al. 1997, ApJ, 486, 126
Leahy, D. A., Darbro, W., Elsner, R. F., Weisskopf, M. C., Sutherland, P. G., Kahn, S. M., & Grindlay, J. E. 1983, ApJ, 266, 160
Leahy, D. A., Harrison, F. A., & Yoshida, A. 1997, ApJ, 475, 823
Maraschi, L., & Treves, A. 1981, MNRAS, 194, 1P
Mushotzky, R., & Jahoda, K. 1992, in The X-Ray Background, ed. X. Barcons & A. C. Fabian (Cambridge Univ. Press)
Peracaula, M. 1997, Ph.D. thesis, Univ. de Barcelona
Press, W. A., Teukolsky, S. A., Vetterling, W. T., & Flannery, B. P. 1992, Numerical Recipes in C (Cambridge: Cambridge Univ. Press)
Ray, P. S., Foster, R. S., Waltman, E. B., Ghigo, F. D., & Tavani, M. 1997, ApJ, 491, 381
Strickman, M. S., Tavani, M., Coe, M. J., Steele, I. A., Fabregat, J., Martí, J., Paredes, J. M., & Ray, P. S. 1998, ApJ, 497, 419
Tavani, M., Arons, J., & Kaspi, V. 1994, ApJ, 433, L37
Tavani, M., Kniffen, D., Mattox, J. R., Parades, J. M., & Foster, R. S. 1998, ApJ, 497, L89
Taylor, A. R., & Gregory, P. C. 1982, ApJ, 255, 210
———. 1984, ApJ, 283, 273
Taylor, A. R., Young, G., Peracaula, M., Kenny, H. T., & Gregory, P. C. 1996, A&A, 305, 817
Turner, T. J., & Pounds, K. A. 1989, MNRAS, 240, 833
van Dijk, R., et al. 1996, A&A, 315, 485
Worrall, D. M., Marshall, F. E., Boldt, E. A., & Swank, J. H. 1992, ApJ, 255, 111

Note added in proof.—Since acceptance of this paper, a refined background model for pointings 1–7 has become available. Reanalysis of the data using this model increases flux measurements between 10%–20%, less than the overall uncertainty in flux zero level. None of the conclusions of the paper are altered.